Lattice dynamics of filled skutterudites: $La(Fe,Co)_4Sb_{12}$

J. L. Feldman, D. J. Singh, and C. Kendziora
Naval Research Laboratory, Washington, D.C. 20375-5345, USA

D. Mandrus and B. C. Sales
Condensed Matter Sciences Division, Oak Ridge National Laboratory, Oak Ridge, Tennessee 37831, USA

(Received 2 December 2002; published 4 September 2003)

Materials for thermoelectric application should have low lattice thermal conductivities. Here we use a comparison of theoretical calculations and Raman spectroscopy to study the lattice dynamics of a La filled skutterudite and identify the Raman active modes. Polarized Raman spectra from polycrystalline $La_{0.75}Fe_3CoSb_{12}$ are presented. First principles calculations of atomic forces generated by small displacements from the ideal skutterudite structure are utilized in a least squares procedure to evaluate the general force constant tensors. These are used to predict the normal mode frequencies and displacement patterns. The relative Raman intensity for each vibration is then estimated using a bond polarizability model. We find that both the centers of gravity of the eight symmetry-allowed Raman peaks and their relative intensities are in excellent agreement with the theoretical predictions. This agreement supports our mode assignments, particularly for those of A_g symmetry, which exhibit a strong polarization dependence. The ''rattling'' vibrations of interstitial La are expected to be Raman inactive for an ideal fully filled material and are not observed.

DOI: 10.1103/PhysRevB.68.094301 PACS number(s): 78.30.−j, 72.20.Pa, 63.20.Dj, 71.15.Nc

I. INTRODUCTION

Materials of the skutterudite structure and the so-called filled skutterudite structure have stoichiometry AB_3, and AB_4C_{12}, respectively, where typically A is a rare earth atom, B a transition metal atom, and C a pnicogen atom. They have a wide range of unusual and potentially technologically important physical properties. In particular the antimonide skutterudites have been the subject of numerous recent studies due to their potential for thermoelectric applications.[1–7] Additionally, some filled skutterudites display superconducting and magnetic transitions as well as rather exotic electronic state properties.[8–11]

The skutterudite structure itself is unusual and may be exploited to obtain materials with good thermoelectric properties. The structural ''filling'' refers to the occupation of interstitial sites (''void'' sites) of the skutterudite structure with no change in space group ($Im\bar{3}$). The prevailing paradigm holds that thermoelectric properties can be optimized by filling the voids with heavy ''rattling'' ions, which are weakly bonded to the lattice.[12] Within this framework, filling is used to frustrate lattice thermal conduction, with the expectation of a minimal effect on electrical properties. While this is likely an oversimplification as regards electrical properties,[13] and while calculations show that the filling atom interacts covalently with the ''host'' atoms,[14] it is observed that filling does indeed substantially reduce the thermal conductivity. For good thermoelectrical properties charge compensation is needed to maintain a semiconducting band structure. Generally it is also found that it is not possible to synthesize single phase materials of an arbitrary composition and that the filling fraction depends on the amount of substitution on the transition metal site. Therefore the filled skutterudites that are of most interest are generally at least quaternary compounds. The thermal conductivity as a function of temperature has been measured for a variety of alloys of varying composition and filling fraction.[4,5,7] It has been demonstrated that chemical disorder on the transition-metal site alone can cause a substantial decrease in thermal conductivity. In materials with nonzero filling fraction, it is found that a factor of 2 decrease in room temperature thermal conductivity comes from transition metal atom substitution, whereas factors of 5 or better come from filler atoms.[4,5] Systematic experimental studies of the partial filling effect on the thermal conductivity[4,6] indicate that the most favorable materials are the partially filled ones. Some evidence has also been given in support of a solid-solution model of partially filled materials.[6,15]

Vibrational studies on skutterudites in the literature include infrared (IR) absorption,[16,17] and Raman[18–20] and inelastic neutron scattering[21,22] experiments as well as a limited number of frozen phonon local density approximation (LDA) calculations[14,23,24] and Born von-Karman modeling calculations.[16,25,26] IR active low frequency modes associated with the filling atom have been identified[17] and the inelastic neutron scattering studies have also provided evidence of low frequency filling atom modes.[21,22] The measured specific heat and LDA calculations have been found to be consistent with some of those measurements as well.[26] Further, large filling atom mean square displacements have been obtained via neutron diffraction studies in the case of several filled skutterudite materials, e.g., see Ref. 27, consistent with the observed frequencies. These studies do not clearly imply strong deviations from harmonic theory, and the simple picture of a rattling atom in a void remains to be established. For a perfect crystal of a filled skutterudite the normal modes are Bloch-like, even those modes with a strong La component, and the thermal conductivity is limited by anharmonicity alone. Perhaps the large mean square displacements of the filling atom can lead to strong anharmonic scattering. Mass disorder effects of partial filling have been considered on the basis of Klemens' Rayleigh scattering treatment with con-

flicting results.[4,6] Not considered thus far for thermal resistance associated with partial filling are resonance (harmonic) scattering effects over a narrow range of phonons.[28] Finally, fully filled skutterudites can also be expected to have some difference in thermal conductivity from unfilled skutterudites simply from the difference in their normal mode dispersion curves.

It is the purpose of this paper to obtain reliable information on the dynamics and interatomic force constants for particular filled skutterudites as a step towards obtaining a better understanding of the thermal transport in these materials. We present and compare first principles (LDA) theoretical results and Raman experimental results for rare-earth-filled skutterudite materials. In particular, experiments were performed on a polycrystalline sample of $La_{0.75}Fe_3CoSb_{12}$ with polarized light and the theory is for $LaFe_4Sb_{12}$. It is not necessarily expected that one should get agreement in the Raman scattering from two such differing materials especially upon noting the above mentioned dependencies of thermal conductivity. On the other hand, we note that the Raman active modes of the perfect crystal exclusively involve vibrations on the Sb sites, for which there is no nominal site disorder in the material of our experimental study. Furthermore, recent specific heat measurements on two nominally fully filled materials, one with Fe_4 and the other with $CoFe_3$ transition metal content, indicate that the lattice dynamical properties of the two materials are similar.[26] Lastly, the measured structural parameters of the sample[27] are quite close to those of the pure material. We shall present data with features that are probably due to the disorder in our sample, but with several features that can be explained in terms of an ordered material. Through our use of both parallel and cross polarization geometry, we are able to identify the two A_g peaks of the spectrum. We compare both Raman frequencies and intensities, although the latter are not calculated from first principles. We use the bond polarizability (BP) model approach in this paper and introduce a BP model for the skutterudite structure to estimate the intensities. Thus both LDA based normal mode frequencies and eigenvectors are utilized. In addition we present the LDA results for the second order force constant tensors limited to zone-center-like displacements as well as for cubic anharmonic central force parameters. The theoretical methods will be discussed in detail in a following section.

II. EXPERIMENTAL DETAILS

The details of sample fabrication and the structural properties have been given in an earlier paper.[27] The nominal composition of the sample is $La_{0.75}CoFe_3Sb_{12}$ and the measured composition is $La_{0.743}Fe_{2.74}Co_{1.26}Sb_{12}$. At room temperature the lattice parameter $a=9.0971(6)$ Å and there are 24 Sb atoms in the conventional cell at the g sites (Wyckoff notation) at $(0,y,z)$ with $y=0.336782(9)$ and $z=0.16021(8)$.

The Raman scattering measurements were performed in pseudobackscattering geometry where the incident laser beam impinged on the sample at an angle of roughly 45° with respect to the surface normal. Scattered radiation was collected within an $f/\#2$ cone normal to the surface. The collected light was dispersed using a triple grating spectrometer in subtractive mode and integrated using an LN_2 cooled CCD array. Both the incident and scattered light were linearly polarized. Where the incoming and outgoing photon polarizations were parallel, the spectra are indicated as *VV*. *HV* indicates that the incoming and outgoing polarizations were orthogonal.

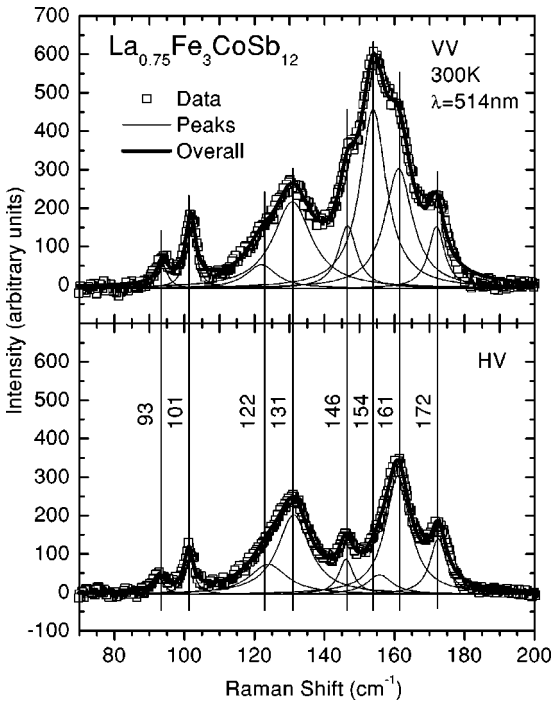

FIG. 1. Experimental Raman spectra for $La_{0.75}Fe_3CoSb_{12}$. *VV* corresponds to parallel polarizations and *HV* to perpendicular polarizations between incident and observed scattered light. Eight Lorentzian functions (thin solid lines) were used to fit the data (open squares).

The sample was measured in an atmosphere of helium gas to avoid rotational lines due to air. Several laser wavelengths were tested to demonstrate that the observed features were due to the Raman process. The data presented were taken using the 514.5 nm line of an Ar^+ ion laser at an ambient temperature close to 300 K. Because the samples are poor thermal conductors, there is some local heating due to the laser. The spectra exhibited a relatively weak temperature dependence that is beyond the scope of the present study.

III. EXPERIMENTAL RESULTS

In Fig. 1 we show the room temperature Stokes Raman spectrum for both *HV* and *VV* polarization. The background ''continuum'' offset has been subtracted using a smooth function in order to simplify the presentation and fitting of the normal modes. The maximum depolarization ratio of a randomly oriented system is expected to be 3:4 for perfectly polarized light.[29] Except for frequencies close to 130 cm^{-1} the depolarization ratio can be easily observed to be markedly less than 1 and, for most frequencies, close to 3/4. The fitted functions shown in the figure are Lorentzians. We observe all eight Raman modes allowed by group theory in *VV*

polarization. We also observe at least seven modes in *HV* geometry. As seen in Fig. 1, we can determine which peaks correspond to the two A_g modes by their markedly weaker intensities in *HV*. The observation of incomplete selection rules for the A_g phonons is an indication of some local disorder within the material. The other likely indication of disorder is the relatively broad peak widths we measure. However, the disorder is not enough to allow violation of the selection rules for the IR-active modes. We did not observe any intensity peaks outside the range of frequency shown. Specifically, we did not observe any Raman activity at the frequencies where IR or acoustic modes are calculated to be present. The parameters of the fits will be given later in order that they may be directly compared with the theoretical quantities determined in this paper.

Finally, the Raman scattering data of Ref. 20 are on nominally very similar composition compounds, $La_xFe_3CoSb_{12}$, as ours. Specifically, Li *et al.*[20] have performed measurements, for parallel polarization, on four samples with x ranging from 0.2 to 0.8. They obtained largely different results from those presented in this paper, although there is some similarity. For $x=0.8$ their data show two strong peaks centered at 157 and 179 cm^{-1} plus very weak structure in the remaining portion of the spectrum. For decreasing values of x, a strong low frequency (90 cm^{-1}) peak becomes prominent as well. Their results clearly differ from ours except for the overall range of frequencies for which there are Raman peaks. Li *et al.* have also interpreted certain features in their data as arising from a small amount of crystalline phases other than the skutterudite structure in their samples. In addition, Raman data on related filled skutterudites[18,19] are largely different from the data of the present work as well.

IV. CALCULATIONAL APPROACH

The space group symmetry operations, as well as the physical constraints of rigid translational invariance and conservative forces,[30] have been used to identify 60 independent second order force constant parameters for the skutterudite structure appropriate to zone-center-like atomic displacements. The rigid rotationally invariant condition provides two additional constraints leading to 58 independent second order force constants required to obtain all of the nonzero frequency zone-center vibrational modes. These latter two constraints were not imposed on the force constant parameters, but we have found that they are approximately obeyed. The direct method has been used to evaluate the parameters. The atomic forces generated by chosen atomic displacements from perfect crystalline geometrical positions of a reference structure (to be discussed below) have been calculated within the local density approximation using the linearized augmented plane wave method.[31] We restrict these displacements to maintain the lattice periodicity; hence the above restriction to zone-center parameters. Our implementation of the direct method differs from some others[32] in that we use a larger number of displacement sets (see the Appendix) than are necessary to obtain values of the independent force constant parameters if one assumes that the above physical constraints are exactly satisfied within the computations and that anharmonicity is negligible. We also chose some displacements to be sufficiently large that cubic anharmonic contributions could be obtained, as discussed in the Appendix. We approximate the form of the cubic anharmonic force contributions to be within the central force leading term[33] approximation. We then perform a least squares fit of the theoretical independent ''data,'' i.e., independent forces, to the usual Taylor series expression. Our results are presented in the form of interatomic force constants, although they are strictly atom-sublattice force constants. We have determined that there are 10 independent sets of atom-sublattice force constant matrices for the filled skutterudite structure of 17 basis atoms (sublattices). In comparison to the process of choosing a minimum number of displacement sets with use of group theoretic methods, our least square method provides a more precise force constant determination. It also allows for a reliable estimate of the computational uncertainties and cubic anharmonic parameters.

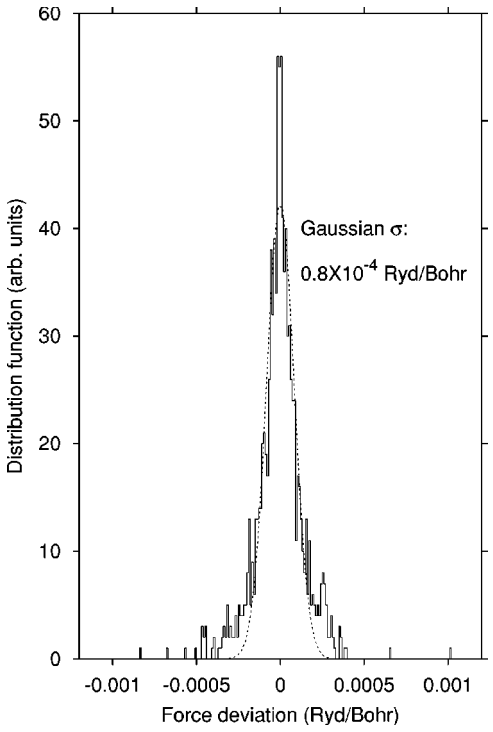

FIG. 2. Distribution function for deviations from least squares fit. The absissa is δf_i (see text). The Gaussian (dashed line) was fit to the distribution function.

In Fig. 2 we plot the distribution of the deviations, δf_i, of the Cartesian force components f_i(LDA), from the fitted Cartesian force components $f_i(fit)$, where the f_i(LDA) are LDA-calculated values and the $f_i(fit)$ are given by the Taylor expansions in the atomic displacements.[30] The plot anticipates the results of the following section. Figure 2 clearly shows the level of the computational uncertainties inherent in our LDA calculations of atomic forces as the range of δf_i is consistent with uncertainties found from (nonzero) values of sums of forces over the unit cell for particular displacement sets and from forces obtained in the reference configuration. The r.m.s., or standard, deviation of the LDA force components is determined to be 0.00014 Ryd/Bohr. This value is used to obtain the uncertainties of the force constant parameters.

TABLE I. Interatomic force constants $-\Phi_{\alpha\beta}(i,j)(10^4$ dyn/cm). The labels i,j are atom labels. The primes indicate that the atom is shifted by a lattice vector from what is shown in Fig. 3. Entries "0" and, e.g., "$-xz$" are a result of space group symmetry, where the latter denotes the negative of the corresponding xz entry. The values in parentheses are standard errors.

i,j	2,15′	11,15	5,6	9,17	6,15′
r	(2.284,0.794,0.818)	(0,0,−2.931)	(2.979,0,0)	(−1.466,0,3.079)	(−1.450,−0.024,3.102)
xx	4.21(6)	0.60(12)	3.66(5)	0.12(1)	0.22(2)
xy	0.62(2)	0	−0.57(4)	0	−0.01(2)
xz	0.85(2)	0	0	−1.27(2)	−0.22(4)
yx	1.10(6)	0	xy	0	−0.05(2)
yy	1.61(2)	0.00(5)	0.28(7)	−0.06(1)	−0.03(3)
yz	0.21(2)	0.03(15)	0	0	−0.20(3)
zx	1.15(6)	0	0	−0.67(2)	−0.95(6)
zy	0.29(2)	$-yz$	0	0	0.04(2)
zz	1.50(2)	4.94(7)	0.25(12)	1.53(1)	1.46(2)
i,j	5,16′	1,17	5,13	1,11′	1,2
r	(−3.079,−1.613,−1.466)	(2.284,2.284,−2.284)	(2.979,2.931,0)	(−2.284,0.794,−3.750)	(4.568,0,0)
xx	0.54(2)	−0.23(1)	0.57(5)	0.36(6)	0.78(5)
xy	0.40(2)	−0.19(1)	0.80(4)	−0.38(2)	−0.28(3)
xz	0.20(4)	0.42(1)	0	−0.27(2)	−0.08(3)
yx	0.37(2)	$-xz$	0	0.25(6)	$-xy$
yy	0.01(3)	xx	0.36(7)	−0.02(2)	0.17(5)
yz	0.16(3)	$-xy$	0	0.23(18)	0.16(3)
zx	0.42(6)	$-xy$	0	−0.22(6)	$-xz$
zy	0.34(2)	xz	0	0.06(2)	yz
zz	−0.01(2)	xx	0.78(12)	0.09(2)	0.11(5)

Finally, let us consider the reference structure used to obtain force constants. Generally the LDA yields a static equilibrium lattice parameter that is a few percent too small compared to experiment. Also, the LDA typically yields best agreement with experiment for normal mode frequencies when the experimental structure is used in the calculations. Therefore, we adopt the room temperature experimental structure of $LaFe_4Sb_{12}$ as our reference structure, i.e., $a=9.136$ Å and Sb x, y, and z coordinate values of 0, 0.33696, 0.16042. We obtain for the LDA force on this Sb site (0,−0.00942,0.0124) Ryd/Bohr. For comparison, we also computed the minimum energy x, y, and z coordinate values to be 0, 0.33416, 0.16422, with the lattice parameter kept fixed at the experimental value. We compare these values to the room temperature experimental values, and see that the differences, i.e., respectively −0.003 and 0.004 for y and z, are small on a scale of where anharmonic effects in the forces become significant, for we used displacements of these sizes in our analysis. Therefore we may expect that the theoretical minimum energy structure would yield effectively identical results to the present ones.

V. RESULTS FOR FORCE CONSTANTS AND VIBRATIONAL SPECTRUM

We present the least squares fitted results for the representative harmonic force constant parameters in Tables I and II. Force constants for interatomic separations related to these by space group operations are of course determined by the appropriate relationships.[30] The atom labels refer to the atoms of Fig. 3. In the tables $-\Phi_{\alpha\beta}(i,j)$ is the α component of the force on atom i generated by a unit displacement, along the β direction, of atom j and **r** is defined as $\mathbf{r}_j-\mathbf{r}_i$. The assumption is made that the forces are appropriately cut off as discussed in the following section. The atom-sublattice force constants, which, strictly, are the quantities obtained through our least square fit, are identical to the values in the table except for the entries in columns labeled 1,17 and 1,2 which are half the atom-sublattice values. As mentioned above, the uncertainties shown in the tables are the standard errors that come from the standard deviation of the LDA "data." Almost all of the quantities of Table I were treated as independent parameters in the least squares procedure; exceptions are the yz elements in the 11,15 and 1,11′ labeled columns that have been expressed in terms of the independent parameters.[34] On the other hand, all of the parameters of

TABLE II. Self force-constants $-\Phi_{\alpha\beta}(i,i)(10^4$ dyn/cm).

Atom	xx	yy	zz	xy	xz	yz
Fe (3)	−17.2(2)	xx	xx	1.6(2)	xy	xy
Sb (11)	−15.1(3)	−10.4(1)	−11.7(2)	0	0	0.2(2)
La (17)	−4.5(1)	xx	xx	0	0	0

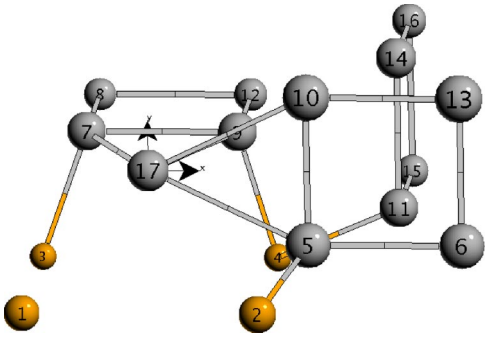

FIG. 3. The 17 atoms that make up the primitive unit cell. The labelings are defined as Fe, 1–4; Sb, 5–16; and La, 17. The *z*-axis points towards the reader. In fractional coordinates atom 17 is at the origin, atom 3 is at (1/4, 1/4, 1/4)–(1/2, 1/2, 1/2), and atom 11 is at (0, 0.337, 0.167)–(-1/2, 1/2, 1/2).

Table II have been expressed in terms of the independent parameters of Table I. The least squares uncertainties given in parentheses are therefore either directly obtained in the least squares fit, in the case of the independent parameters, or cumulative, in the case of the dependent parameters.

The fitted cubic anharmonic central force parameters are given in Table III. Note that there are no entries corresponding to Fe-Fe and La-Fe. There are only eight values, contrasted with the fact that there are ten interatomic pairs for which second order force constants were obtained. Indeed it can be shown that forces generated by zone center displacement sets cannot provide any information on odd order anharmonic coefficients that do not involve Sb. This is related to the fact that La and Fe sites are inversion centers plus the fact that under inversion these sites go into equivalent ones via a lattice translation.

Table I shows that the magnitudes of the harmonic force constants appear to rapidly decrease after the lowest few interatomic distances and then to level off to values less than one fifth of the largest values. A somewhat larger computational cell than the primitive unit cell is probably necessary for an accurate determination of interatomic force constants. In assessing our results it is useful to specify the nearest and next nearest neighbor distances corresponding to each of the representative basis atom pairs. In principle, each force constant of the table is contributed to by individual interatomic force constants from nearest-neighbor, next-nearest-neighbor, etc., atoms associated with a particular sublattice. For example $\Phi_{xx}(2,15')$ is strictly the force on atom $i=2$ due to identical displacements of an atom at a distance 2.55, one at a distance 5.77, etc. We expect that the forces are short ranged. Therefore we generally expect that the contribution to the force from the atom at the distance 5.77 is considerably smaller than that from the atom at 2.55, but of course the results may also be dependent on the particular Cartesian components considered. In the following, nearest-neighbor and next-nearest-neighbor distances are separated by hyphens and given in the same order as the quantities in Table I: 2.55-5.77, 2.93-6.20, 2.98-6.16, 3.41-5.72, 3.44-5.68, 3.77-4.54, 3.96-7.58, 4.18-5.10, 4.46-4.49, 4.57-6.46 Å. Note that two second-neighbor distances (4.54 and 4.49) are smaller than the largest, 4.57, of the first-neighbor distances. This demonstrates an idiosynchratic feature of the interatomic force constant ''model.'' Possibly certain of our interatomic force constant values would be more meaningful if we had included more distant atoms in the fit, but restricted the matrix form to be in accord with central forces.

TABLE III. Cubic anharmonic parameters, $r\phi'''$, and corresponding interatomic distances, r.

(i,j)	r(Å)	$-r\phi'''$ (10^4 dynes/cm)
(2,15′)	2.553	90.8(3.5)
(11,15)	2.931	49.1(7.9)
(5,6)	2.980	42.8(8.0)
(9,17)	3.410	29.2(1.0)
(6,15′)	3.442	14.1(3.9)
(5,16′)	3.772	15.0(2.2)
(5,13)	4.180	−3.4(9.0)
(1,11′)	4.462	2.2(5.1)

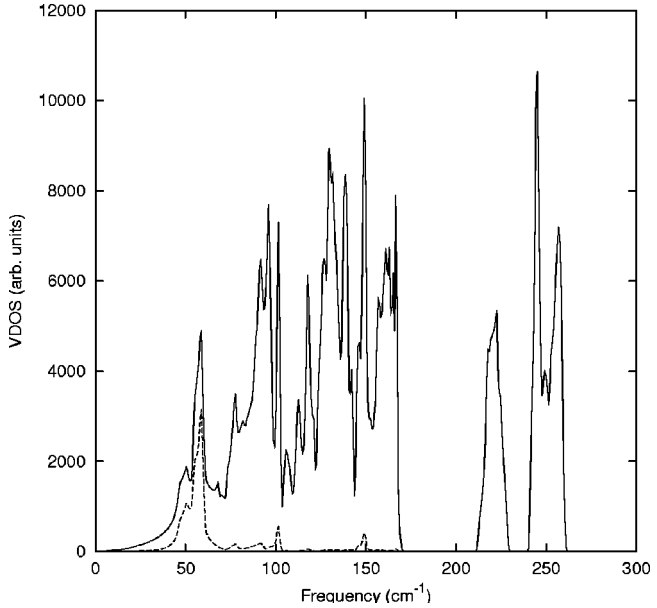

FIG. 4. Calculated vibrational density of states (VDOS): Total VDOS (solid) and La projected VDOS (dashed).

We have calculated the vibrational density of states (VDOS) on the basis of our interatomic force constant results. The results shown in Fig. 4 were based on a grid of 11 726 points in the irreducible portion of the Brillouin zone as well as a Gaussian of FWHM=1 cm^{-1}. These results improve upon our previous calculations[35] which only partially made use of LDA results. There are clear quantitative differences between the two calculations. For example, the strong low frequency La-motion dominated peak is much narrower than for the previous calculation. However, unchanged from the previous paper, is the conclusion that there are normal mode hybridization effects in the rare-earth weighted VDOS that seem consistent with inelastic neutron scattering results.

Insight into the nature of the high frequency vibrations is gained by diagonalizing the Fe self-force-constant matrix, the results of which yield the effective Einstein vibrational

TABLE IV. Zone center frequencies ν and Raman intensities I. Experimental results are parameters of Lorentzian fits to the Raman data (see text). The theoretical intensities are bond polarizability model results. The La force constant effects on the frequencies is represented as the difference $\delta\nu \equiv \nu_{\text{empty}} - \nu$. Frequency units are cm^{-1}

	Theory				Experiment			
Rep.	ν	I (VV)	I (HV)	$\delta\nu_{\text{empty}}$	ν	I (VV)	I (HV)	Width
F_u	54.0(1.3)							
A_u	91.7(5.0)			8.3				
F_u	94.0(1.2)			−14.5				
F_g	95.1(1.6)	0.085	0.066	−10.5	93.8	0.053	0.037	3.5
F_g	101.1(1.2)	0.092	0.071	−2.1	101.8	0.143	0.081	3.4
F_u	119.5(1.1)			−1.2				
E_u	124.8(2.5)			−0.4				
E_g	133.5(1.7)	0.377	0.270	−14.3	122.0	0.154	0.239	10.6
F_g	136.9(1.9)	0.711	0.552	−8.3	130.8	0.701	0.540	13.2
F_u	139.6(0.8)			−11.0				
A_g	148.2(1.8)	0.281		−13.2	146.5	0.248	0.110	6.3
F_u	151.2(1.0)			−0.9				
A_g	155.9(1.8)	1.000		4.5	153.9	1.000	0.106	9.0
E_g	157.6(1.5)	0.784	0.562	4.1	161.2	0.714	0.625	9.6
F_g	164.3(1.6)	0.013	0.010	0.3	172.0	0.218	0.199	5.6
A_u	211.9(3.4)			11.0				
F_u	223.3(2.6)			7.9				
F_u	240.8(2.1)			0.8				
E_u	251.4(2.3)			−1.9				
F_u	258.8(2.1)			−1.7				

modes corresponding to the Fe atoms. The results are a frequency of 239 cm^{-1}, corresponding to doubly degenerate modes, and one at 206 cm^{-1}, corresponding to Fe motion along the (trigonal) La-Fe axis. The VDOS shows two major peaks with a ratio of 1/2 for the areas under the peaks and a split upper peak. Clearly, the two peaks correspond to different directions of Fe motion; the breadths and splittings correspond to dynamical effects associated with Sb motion. Our results are also in excellent agreement with neutron data over the whole spectrum,[36] with account taken of the instrumental resolution. Furthermore, these results have implications for the Fe mean square displacements. The fact that the lower (frequency) peak corresponds to motion primarily along the trigonal axis which is toward the rare earth site means that the mean square displacement is greatest along the trigonal axis within harmonic theory. That result has also been observed experimentally.[27]

Finally, it is interesting to compare the calculated VDOS with the measured Raman spectra of Fig. 1. The shapes of the spectra in the Raman region are substantially different except for the region of the depletion of modes near 110 cm^{-1}. The results are roughly consistent with the ordinarily weaker coupling to the field of low frequency modes in comparison to high frequency modes. It is also emphasized that despite the substitutional and partial filling nature of our sample there is no obvious leakage of possible infrared active modes—either high frequency transition-metal modes or low frequency La modes.

VI. ZONE CENTER NORMAL MODE PROPERTIES

In this section we concentrate on the zone center normal mode properties that are obtained with no additional approximation than the LDA, namely, the frequencies and eigenvectors and we discuss the comparison with the Raman-peak frequencies. The LDA often achieves roughly 10–20 % accuracy in phonon frequencies, but in addition there always exist computational uncertainties. In Table IV we present all of the zone center frequencies as well as Raman scattering results. The computational uncertainties, which are the values in parentheses, were calculated from the force constant uncertainties presented in Table I using standard error analysis and we see that aside from the 5% uncertainty for the low frequency A_u mode the frequencies are precise to 2% or better. The most careful comparison between theory and experiment can be achieved for the A_g modes since they have been identified experimentally by the *HV-VV* comparison. The observed 1% agreement is well within theoretical error estimates, but there is a caveat, as we cannot measure the polarization vectors and conceivably the characters of the two A_g modes could be reversed from what we claim theoretically. The group theoretical symmetries of the remaining Raman modes have not been identified experimentally because of the polycrystalline nature of the sample. The unique identification of each mode experimentally would require single crystal samples with site specific isotopic substitutions. If we assume that the theory correctly gives the frequency ordering of the symmetries—and the placements of

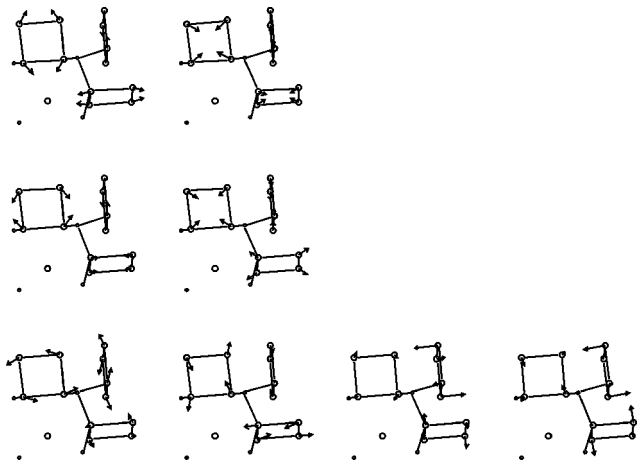

FIG. 5. Raman active modes. The top two are A_g, the middle two E_g, and the bottom four F_g. For each symmetry type the modes are ordered according to frequency with the lowest frequency mode at the left. The structure is rotated with respect to Fig. 3. For clarity no bonds are shown connecting the La atom to its neighboring Sb atoms.

the A_g modes with respect to the other modes seem to be consistent with that assumption—then, with only one exception, the agreement between theory and experiment is seen to be better than 5%.

Within our force constant ''model,'' the effect of the presence of the La atom on the zone center frequencies is also given in this table. We present values of $\nu_{\text{empty}}-\nu$. Here ν_{empty} is obtained by recalculating the frequencies for a modified dynamical matrix whereby the La contributions are omitted.[37] This has some bearing on our comparison of theory and experiment. The frequencies calculated for the fully filled material would be modified somewhat in a true calculation of Raman peaks of a 75% partially filled material. Very roughly, one might expect a shift in calculational frequency of about $0.25\delta\nu_{\text{empty}}$. Of course, partial filling can have other effects on the lattice dynamics than those given by this simple estimate. Furthermore anharmonicity associated with large amplitude La atom vibrations at room temperature could also be important for Raman-peak frequencies. Let us next briefly consider the Raman widths given in the table. Generally they are seen to be larger than Raman widths measured for pure unfilled materials. We believe that structural disorder contributes to those widths and certainly our simple model for the effect of the La force constants on the frequencies is suggestive of that fact. However, a rigorous treatment within our force constant results such as a supercell calculation or a coherent potential approximation calculation might shed light on our results for the peak widths. Such calculations are outside the scope of this paper.

The normal modes are depicted in Figs. 5–7, where only one mode of each set of degenerate modes is shown. We emphasize that what are depicted are the actual normal mode patterns—not the eigenvectors, which are related to the atomic displacements by mass factors. The modes are arranged according to irreducible representation and to frequency as described in the figure captions, where the leftmost mode is the lowest frequency of a symmetry type. The

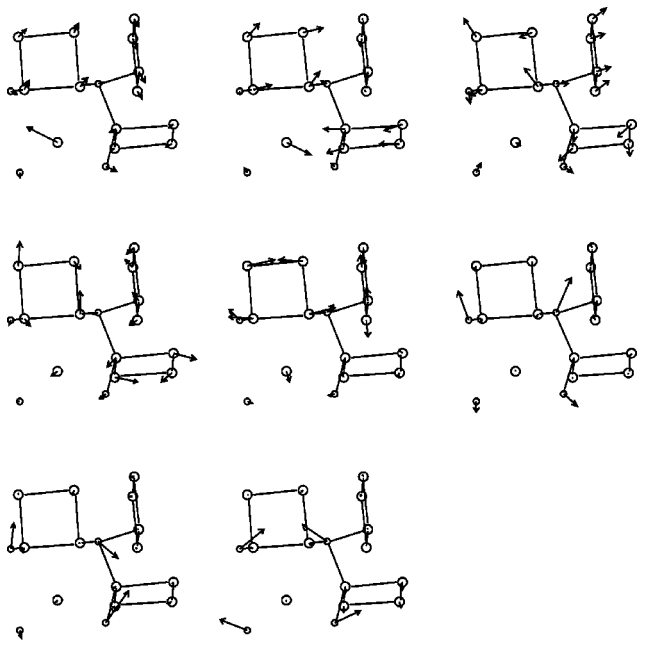

FIG. 6. Infrared active (F_u) modes. The top modes are lowest in frequency and the frequency increases consecutively from left to right. The structure is rotated with respect to Fig. 3. For clarity no bonds are shown connecting the La atom to its neighboring Sb atoms.

modes of Figs. 5, 6, and 7 are, respectively, the Raman active, infrared active, and optically silent modes. Figure 6 depicts the F_u modes, all of which are infrared active, and Fig. 7 depicts the A_u and E_u modes that are optically silent.

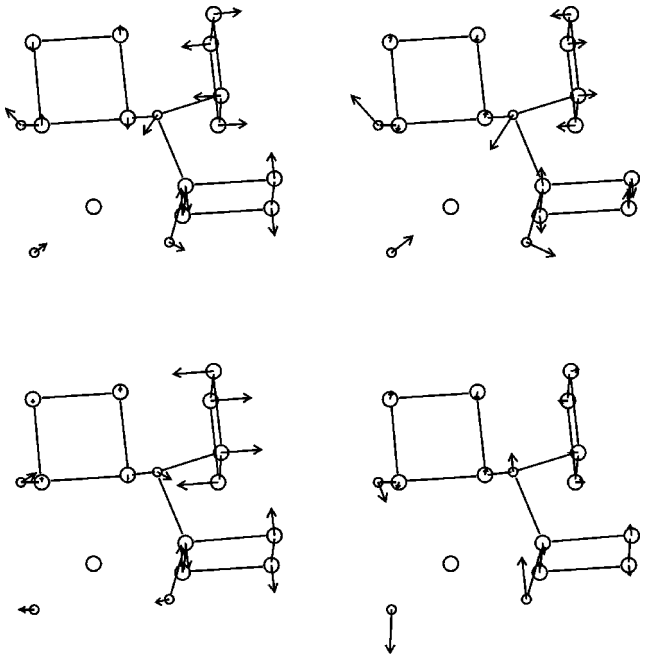

FIG. 7. Optically silent modes. The top two modes are A_u and the bottom two E_u, with frequency ordering such that the lowest frequency mode of each symmetry is at the left. The structure is rotated with respect to Fig. 3. For clarity no bonds are shown connecting the La atom to its neighboring Sb atoms.

The figures show that the modes fall into several classes as a result of the atomic masses as well as the disparity of the values of force constants. For example, consider the differences between values of inter-ring and intraring Sb-Sb force constants of Table I. The Raman active, or *g*-symmetry modes involve only Sb motion and are in the low frequency regime by virtue of the relative masses of Fe and Sb. The *u*-symmetry modes cover the full spectrum of zone-center modes, where the higher frequency modes are mainly Fe vibrations and are separated by a substantial gap in frequency from the remaining modes. La motion occurs only in the F_u (infrared active) modes and substantially only in the two lowest frequency modes. Other features of the modes are also displayed in the figures. The highest frequency A_g mode is the one which most strongly affects the areas of the Sb rings. There are also quasi rigid-ring modes, quasi in-plane and out-of-plane modes (to the planes of the Sb rings), and Sb-Sb shearing and stretching modes.

VII. COMPARISON OF RAMAN INTENSITIES

It is worthwhile to apply the information on the eigenvectors that we obtained to a calculation of the Raman intensities in order to gain confidence in our mode assignment. The expression for the Stokes Raman intensity within the harmonic approximation is

$$I_{\eta',\eta}(\omega_L-\omega_S)\propto\omega_L\omega_S^3\sum_{f=1}^{3N}\frac{n(\omega_f,T)+1}{\omega_f}|\eta'_\alpha\eta_\beta P_{\alpha\beta,f}|^2 \times\delta(\omega_L-\omega_S-\omega_f). \quad (1)$$

In this expression, f is a normal mode label, ω_f is a normal mode frequency, n is the phonon occupation at temperature T, and $P_{\alpha\beta,f}$ is the derivative of the electronic polarizability tensor with respect to a normal coordinate. The relevant laser light properties given in this expression are respectively the incident and scattered frequencies, ω_L and ω_S, and the incident and scattered polarization directions, given by unit vectors $\boldsymbol{\eta}$ and $\boldsymbol{\eta}'$. The quantities $\boldsymbol{\eta}$ and $\boldsymbol{\eta}'$ are parallel (perpendicular) vectors for *VV* (*VH*) geometries. The areas under the Raman peaks are identified with the integrals of the above expression with respect to the frequency shift ω_L-ω_S and we refer to them as *intensities* in the following discussion. The basic premise of a bond polarizability (BP) model is that the polarizability tensor $P_{\alpha\beta}$ is determined from a linear superposition of independent, diatomic molecule, bond polarizability tensors. We employ the general BP model expressions of Ref. 38 for $P_{\alpha\beta,f}$ in terms of normal mode displacement patterns and BP parameters. Based on our electronic band theoretic knowledge[14,39] of the skutterudites the bonds that ought to be considered are those between nearest-neighbor Fe and Sb atoms and those between Sb atoms on the sides of the rectangular Sb rings. For each bond one introduces parameters for the bond-length-derivitives of the isotropic and anisotropic components of the bond polarizability tensor, respectively, $\alpha'_\parallel+2\alpha'_\perp$ and $\alpha'_\parallel-\alpha'_\perp$ and a parameter for the anisotropic component itself $\alpha_\parallel-\alpha_\perp$. In our case, there are nine parameters and eight Raman intensities to be fit, but there is an admittedly loosely defined range of acceptable values of parameters. Lefebvre-Devos *et al.*[39] considered the nature of the bonds for $CoSb_3$ on the basis of electronic structure calculations, as well as of x-ray absorption and Sb Mossbauer experiments. They proposed that the bond strengths between neighboring Sb's and between nearest-neighbor Sb and Co atoms are very similar and that there is a stronger Sb-Sb bond for the shorter length on the Sb rectangular ring, as is also consistent with our force constant results (see Table I). We wish to obtain results that are consistent with these observations. We have performed a trial-and-error analysis using various choices of parameters. The input into these calculations was our LDA eigenvectors and frequencies. The calculations also required the use of polycrystalline averages of expression (1) in order to be consistent with the nature of the sample. The calculation was performed for room temperature. We found that for most choices, obviously unphysical values of the parameters gave quite poor results for the intensities, whereas physically reasonable ones, i.e., comparable values for Sb-Sb and Sb-Fe parameters, gave the best results. However, we were unable to fit the highest frequency peak intensity simultaneously with the other seven within these constraints.

TABLE V. Parameters for the bond polarizability model. Subscript 1 (2) refers to longer (shorter) bond length.

	Sb-Fe	$(\text{Sb-Sb})_1$	$(\text{Sb-Sb})_2$
$\alpha'_\parallel-\alpha'_\perp$	1.0	0.85	1.0
$\alpha'_\parallel+2\alpha'_\perp$	1.7	1.44	1.7
$(\alpha_\parallel-\alpha_\perp)/r_{ij}$	−0.5	−0.75	−0.5

We performed the polycrystalline averages numerically with the use of Euler angles, although the analytic expressions for the Raman intensity of randomly oriented materials in parallel and cross polarization geometries are available.[40] The sensitivity of the results to the number of random orientations was explored, but only results that are sufficiently ''polycrystalline,'' in the sense that the 3:4 ratio *HV*:*VV*, is well satisfied, are given: For the polycrystalline average of a cubic crystal, the maximum depolarization ratio (*HV*:*VV*) of 3:4[29] is expected for modes other than the A_g modes, which yield zero depolarization ratio. The final results are shown in Tables IV (intensities) and V (bond polarizability parameters). Since absolute intensities have not been measured, only relative quantities are given in these tables, and the values for I (*VV*) corresponding to the high frequency A_g mode are set to unity for purposes of comparison. The agreement between theory and experiment is good, supporting the mode assignments as well as the bond polarizability calculations. The results are also quite plausible. For example, the breathing type modes of A_g and E_g symmetry (see Fig. 5) yield the largest intensities. A large discrepancy occurs only for the highest frequency mode. In view of the simplicity of our bond polarizability model it is not surprising that there is some deviation between theory and experiment. In particular we would expect a sensitivity to the inclusion of more distant bonds than those treated here as well as to a slightly more sophisticated model for the bond polarizability tensor associated with the Sb-Sb bonds that are included. We have also

not attempted to fit the Lorentzians to the data such that the 3:4 rule for the intensity ratios is most closely obeyed. This is particularly evident for the low frequency ($122\ cm^{-1}$) E_g mode for which the intensity in *HV* geometry is much larger than in *VV* geometry, an apparently anomalous result. Nevertheless, the *VV* and *HV* intensities in that spectral region are comparable to each other, and therefore either the Lorentzian fits have a large uncertainty due to overlap of peaks or perhaps the appropriate shapes of the peaks may deviate from Lorentzians. Furthermore, the low frequency E_g peak is the only peak for which the LDA calculation does not give the frequency to better than a few percent accuracy.

VIII. SUMMARY AND CONCLUSIONS

We have studied the lattice dynamics of $La_{0.75}Fe_3CoSb_{12}$ through polarized Raman spectroscopy and first principles calculations of interatomic forces based on the ideal composition $LaFe_4Sb_{12}$. By comparing crossed and parallel polarizations, we have experimentally identified the Raman modes of A_g symmetry. The results of the first principles calculations were also adapted into a bond polarizability model for the prediction of Raman intensities for the ideal composition. The strong agreement of our predicted frequencies and intensities with experiment suggests that the crystalline model is useful for describing the main features of the experimental results. The combined relationship of frequency and Raman intensity gives us some confidence in the assignment of the other six modes. However, features of the experimental results such as the leakage of A_g symmetry in cross polarization and large broadening of Raman peaks is outside the scope of our theoretical treatment, except for the fact that our calculated force constants might be used to model a disordered structure. Toward that end we have also computed the zone center frequencies without the La force constants to estimate the effect of incomplete filling. It is also possible that the broadening is a dynamical effect associated with the filling atom, as suggested in other works.[18–20]

Some of the aspects of the theoretical methods are also worth mentioning. More than 1000 LDA atomic force components were obtained and these were used in a least squares fitting procedure to obtain not only all of the independent harmonic force constant values (within the limits of the zone center displacement method) but their least squares uncertainties as well. These calculational uncertainties, which do not take account of systematic errors of the LDA, were found to be less than two percent for the strongest force constants. The force constants were found to decrease, overall, with increasing interatomic distance but force constants outside our maximum 4.5 Å interatomic distance cannot be neglected. The results partially support simpler model results, which have dominant nearest-neighbor force constants and large central force components. In addition, we have extracted effective cubic anharmonic central force parameters. The cubic anharmonic La-Sb central force parameter is sizeable, and we expect that these values could find use in future theoretical treatments of thermal conductivity as well as of other anharmonic properties.

We have applied our force constant results to a calculation of both the full vibrational density of states and the La weighted vibrational density of states. The latter is sharply peaked at a low frequency and has small components at higher frequencies. These results can be compared to previous less rigorous results.[35] The La weighted low frequency peak is seen to be narrower than previously calculated, but the overall agreement with the results of an analysis of inelastic neutron scattering data remains.[21,26]

Finally, our lattice dynamical results can be used to reliably estimate several equilibrium vibrational and thermal properties, especially those that are primarily describable within the harmonic approximation, such as dispersion curves, specific heat, and Debye Waller factors. They could also be a basis for calculations of thermal conductivity. The description of the lattice dynamics given here is a necessary ingredient to a Boltzmann-Peierls approach. We have also given an estimate of cubic anharmonic parameters which enter into such an approach. With additional considerations to those which we have made, our results might also be applicable to a (classical) Green-Kubo calculation of the type performed for a clathrate by Dong *et al.*[41] Finally the partial filling effect might also be taken into account employing our La-based force constants. Note that in the case of partial filling, resonant scattering in the harmonic approximation can reduce thermal conductivity, although some anharmonicity is required in principle to achieve finite thermal conductivity.

ACKNOWLEDGMENTS

We thank Dr. M. J. Mehl for providing us with the uniform grids in the irreducible portion of the Brillouin zone for calculating the vibrational density of states. We are grateful for helpful discussions with T. Caillait, J. P. Fleurial, J. Dong, and G. Slack. The work at NRL is supported by the Office of Naval Research. Oak Ridge National Laboratory is managed by UT-Battelle LLC for the U.S. Department of Energy under Contract No. DE-AC05-00OR22725.

APPENDIX: TYPES OF DISPLACEMENT SETS

Atoms within the unit cell are displaced in three different ways. In one way (type 1), displacement sets of rhombohedral-like distortions were used. (The point group symmetry is reduced to C_3.) This entailed seven atom types within the unit cell with a La and an Fe (Fe-1) on the trigonal axis, and an Fe (Fe-2) and four Sb atoms in general positions, yielding seventeen independent force components. We also used displacement sets consistent with the La atoms displaced along one of the cubic axes yielding orthorhombic symmetry (type 2). (The point group is reduced to C_{2v}.) Within this reduced symmetry seven atom types are again found; the La atom, a single Fe atom, and five Sb's, where the La is restricted to a single direction (z), one of the Sb atoms and the Fe atom is in a general position, and the remaining Sb's are confined to the *xz* and *yz* planes. This gives fifteen independent force components for each set of displacements. Finally several calculations were done for a gen-

eral set of displacements whereby 51 independent force parameters resulted from a single displacement set (type 3). The cost in time of the LDA calculations depended on the symmetry employed, and we obtained much more data from the type 1 calculation than from the others.

From thirty nine LDA calculations of type 1, 663 force components are obtained. Nevertheless the much smaller number of independent harmonic force constants cannot be entirely determined from this information alone because of the rhombohedral symmetry restriction. Thus there is much redundancy in this information. By including five displacement sets of type 3 and six of type 2, we are able to completely determine all independent harmonic force constants within a least squares procedure. A total of 1044 independent force components comprised our ''data'' set.

As a specific example of our choice of displacement sets of type 1, in sixteen separate calculations we displaced each of the four distinct Sb atoms along each of the cubic body diagonals by an amount $0.00433a$. The remaining sets of displacements involved either a variety of combinations of atoms or separate displacements of Fe-1 and La atoms along the trigonal axis.

Two calculations were also performed for substantially larger La displacements, of $0.02a$ and $0.04a$, along one of the cubic axes (type 2) as compared to all other displacements that we chose. These displacements provide information on both cubic and quartic anharmonic potential energy terms and will be discussed in detail in a subsequent paper. However, we have included the $0.02a$ data set in our analysis (with no correction for the quartic anharmonic terms) in order to achieve the most precise results for the ''bare'' La frequency of Ref. 26: The results are 69.5 and 74.4 cm^{-1} without and with the $0.02a$ displacement set, respectively, to be compared with 74.0 cm^{-1} of Ref. 26.

[1] T.M. Tritt, G.S. Nolas, G.A. Slack, A.C. Ehrlich, D.J. Gillespie, and J.L. Cohn, J. Appl. Phys. **79**, 8412 (1996).

[2] B.C. Sales, D. Mandrus, and R.K. Williams, Science **272**, 1325 (1996).

[3] D.A. Gajewski, N.R. Dilley, E.D. Bauer, E.J. Freeman, R. Chau, M.B. Maple, D. Mandrus, B.C. Sales, and A.H. Lacerda, J. Phys.: Condens. Matter **10**, 6973 (1998).

[4] G.S. Nolas, J.L. Cohn, and G.A. Slack, Phys. Rev. B **58**, 164 (1998).

[5] D.T. Morelli, G.P. Meisner, B. Chen, S. Hu, and C. Uher, Phys. Rev. B **56**, 7376 (1997).

[6] G.P. Meisner, D.T. Morelli, S. Hu, J. Yang, and C. Uher, Phys. Rev. Lett. **80**, 3551 (1998).

[7] B. Chen, J-H. Xu, C. Uher, D.T. Morelli, G.P. Meisner, J.P. Fleurial, T. Caillot, and A. Borshchevsky, Phys. Rev. B **55**, 1476 (1997).

[8] I. Shirotani, T. Uchiumi, K. Ohno, C. Sekine, Y. Nakazawa, K. Kanoda, S. Todo, and T. Yagi, Phys. Rev. B **56**, 7866 (1997).

[9] N. Takeda and M. Ishikawa, J. Phys. Soc. Jpn. **69**, 868 (2000).

[10] E. Bauer, St. Berger, Ch. Paul, M. Della Mea, G. Hilscher, M. Reissner, W. Steiner, A. Grytsiv, P. Rogl, and E.W. Scheidt, Phys. Rev. B **66**, 214421 (2002).

[11] H. Sato, Y. Aoki, T. Namiki, T.D. Matsuda, K. Abe, S. Osaki, S.R. Saha, and H. Sugawara, Physica B **328**, 34 (2003).

[12] G.A. Slack and V.G. Tsoukala, J. Appl. Phys. **76**, 1665 (1994).

[13] D.J. Singh and I.I. Mazin, Phys. Rev. B **56**, 1650 (1997).

[14] L. Nordstrom and D.J. Singh, Phys. Rev. B **53**, 1103 (1996).

[15] F. Grandjean, G.J. Long, R. Cortes, D.T. Morelli, and G.P. Meisner, Phys. Rev. B **62**, 12 569 (2000).

[16] H.D. Lutz and G. Kliche, Phys. Status Solidi B **112**, 549 (1982); H.D. Lutz and G. Kliche, Infrared Phys. **24**, 171 (1984); H.D. Lutz and G. Kliche, J. Solid State Chem. **40**, 64 (1981).

[17] S.V. Dordevic, N.R. Dilley, E.D. Bauer, D.N. Basov, M.B. Maple, and L. Degiori, Phys. Rev. B **60**, 11321 (1999).

[18] G.S. Nolas, G.A. Slack, T. Caillat, and G.P. Meisner, J. Appl. Phys. **79**, 2622 (1996).

[19] G.S. Nolas and C.A. Kendziora, Phys. Rev. B **59**, 6189 (1999).

[20] L.X. Li, H. Liu, J.Y. Wang, X.B. Hu, S.R. Zhao, H.D. Jiang, Q.J. Huang, H.H. Wang, and Z.F. Li, Chem. Phys. Lett. **347**, 373 (2001).

[21] V. Keppens, D. Mandrus, B.C. Sales, B.C. Chakoumakos, P. Dai, R. Caillat, and A. Borchevski, Nature (London) **395**, 876 (1998).

[22] R.P. Hermann, R.J. Jin, W. Schweika, F. Grandjean, D. Mandrus, B.C. Sales, and G.J. Long, Phys. Rev. Lett. **90**, 135505 (2003).

[23] D. J. Singh, M. Fornari, J. L. Feldman, and I. I. Mazin, in *Proceedings of the Eighteenth International Conference on Thermoelectrics* (Ref. 35), p. 448.

[24] M. Fornari and D.J. Singh, Phys. Rev. B **59**, 9722 (1999).

[25] J.L. Feldman and D.J. Singh, Phys. Rev. B **53**, 6273 (1996); **54**, 712(E) (1996).

[26] J.L. Feldman, D.J. Singh, I.I. Mazin, D. Mandrus, and B.C. Sales, Phys. Rev. B **61**, R9209 (2000).

[27] B.C. Chakoumakos, B.C. Sales, D. Mandrus, and V. Keppens, Acta Crystallogr., Sect. B: Struct. Sci. **55**, 341 (1999).

[28] A. A. Maradudin, E. W. Montroll, G. H. Weiss, and I. P. Ipatova, in *Solid State Physics: Advances in Research and Applications*, edited by H. Ehrenreich, F. Seitz, and D. Turnbull (Academic Press, New York, 1971), Suppl. 3, p. 381, and references therein.

[29] D. Bermejo and M. Cardona, J. Non-Cryst. Solids **32**, 405 (1979).

[30] G. Liebfried and W. Ludwig, *Solid State Physics*, edited by F. Seitz and D. Turnbull (Academic Press, New York, 1961).

[31] D. J. Singh, *Planewaves, Pseudopotentials and the LAPW Method* (Kluwer, Boston, 1994); Phys. Rev. B **43**, 6388 (1991).

[32] S.W. Wei and M.Y. Chou, Phys. Rev. B **50**, 2221 (1994); G.A. de Wijs, C.M. Fang, G. Kresse, and G. de With, *ibid.* **65**, 094305 (2002), and references therein; J. Dong, O.F. Sankey, and G. Kern, *ibid.* **60**, 950 (1999); J. Dong and O.F. Sankey, J. Appl. Phys. **87**, 958 (2000); J. Phys.: Condens. Matter **11**, 6129 (1999).

[33] A.A. Maradudin, P.A. Flinn, and R.A. Coldwell-Horsfall, Ann. Phys. (N.Y.) **15**, 360 (1961).

[34] The self-force constant tensors must be symmetric by the conservative force condition and only for the case of La does crystal symmetry impose that. Therefore in order to obtain the required result for Fe and Sb, additional relations among the interatomic force constants are implied.

[35] J.L. Feldman, D.J. Singh, and I.I. Mazin, in *Proceedings of the Eighteenth International Conference on Thermoelectrics*, Baltimore, MD (IEEE, Piscataway, NJ, 1999), p. 9.

[36] V. Keppens, D. Mandrus, B.C. Sales, and P. Dai (unpublished).

[37] However, the self force-constants for Fe and Sb, and the values of the *yz* components for the 11-15 and 1-11 interactions shown in Table I are altered from their values in the La-filled material as they are partially dependent on the La interactions.

[38] S. Guha, J. Menendez, J.B. Page, and G.B. Adams, Phys. Rev. B **56**, 15 431 (1997); P. Umari, A. Pasquarello, and A. Dal Corso, *ibid.* **63**, 094305 (2001).

[39] I. Lefebvre-Devos, M. Lassalle, X. Wallart, J. Olivier-Fourcade, L. Monconduit, and J.C. Jumas, Phys. Rev. B **63**, 125110 (2001).

[40] P.M. Rafailov, V.G. Hadjiev, H. Jantoljak, and C. Thomsen, Solid State Commun. **112**, 517 (1999); W. Hayes and R. Loudon, *Scattering of Light by Crystals* (Wiley, New York, 1978), p. 113.

[41] J. Dong, O. Sankey, and C.W. Myles, Phys. Rev. Lett. **86**, 2361 (2001).